Langmuir

LETTER

pubs.acs.org/Langmuir

Viscoelastic Property Mapping with Contact Resonance Force Microscopy

J. P. Killgore,*,† D. G. Yablon,‡ A. H. Tsou,‡ A. Gannepalli,§ P. A. Yuya,∥,⊥ J. A. Turner,∥ R. Proksch,§ and D. C. Hurley†

†National Institute of Standards and Technology, Boulder, Colorado 80305, United States

‡Corporate Strategic Research, ExxonMobil Research and Engineering, Annandale, New Jersey 08801, United States

§Asylum Research, Santa Barbara, California 93117, United States

∥Department of Engineering Mechanics, University of Nebraska, Lincoln, Nebraska 68588, United States

ABSTRACT: We demonstrate the accurate nanoscale mapping of near-surface loss and storage moduli on a polystyrene−polypropylene blend with contact resonance force microscopy (CR-FM). These viscoelastic properties are extracted from spatially resolved maps of the contact resonance frequency and quality factor of the AFM cantilever. We consider two methods of data acquisition: (i) discrete stepping between mapping points and (ii) continuous scanning. For point mapping and low-speed scanning, the values of the relative loss and storage modulus are in good agreement with the time−temperature superposition of low-frequency dynamic mechanical analysis measurements to the high frequencies probed by CR-FM.

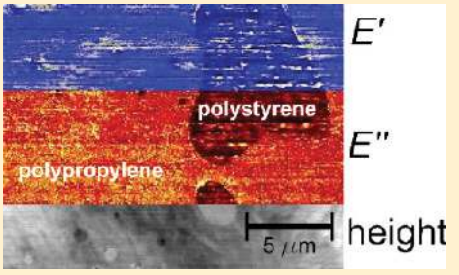

INTRODUCTION

The development of new polymeric materials with heterogeneous micrometer- and nanometer-sized domains requires novel characterization tools to resolve mechanical properties on commensurate length scales. The high spatial resolution of the atomic force microscope[1] (AFM) uniquely positions it to provide mechanical information on these small length scales.[2,3] A number of AFM-based techniques have been developed to extract contrast from mechanical properties. This includes dynamic techniques such as phase imaging[4] and quasistatic techniques such as force−distance spectroscopy.[5] In general, dynamic tapping-based techniques are still limited in their ability to provide accurate quantitative nanomechanical results.[6] However, quantitative approaches such as force−distance spectroscopy afford limited stiffness sensitivity and are typically poorly suited for imaging.[5] Recent efforts have sought to address these limitations,[7−10] but the need still remains to develop accurate, quantitative techniques for AFM-based mechanical characterization.

For polymeric materials, viscoelastic phenomena such as creep, stress relaxation, and the dynamic response can play a critical role in determining the material's ultimate applications. A variety of AFM-based techniques have been used to characterize viscoelastic behavior on the nanoscale,[11,12] including intermittent contact (tapping or amplitude modulation) mode,[13] force modulation,[14,15] force−distance spectroscopy,[16,17] and friction force microscopy.[18,19] For techniques such as intermittent contact mode[13] and force modulation,[14,15] the cantilever's amplitude and phase when oscillated in proximity to a surface determine its conservative and dissipative interactions, which can be correlated to the viscoelastic response if correctly interpreted. Force−distance spectroscopy allows for indentation-type measurements of viscoelasticity by varying the loading rate[16] or by introducing programmed tip−sample dwell periods.[17] Friction force microscopy measures viscoelastic relaxation spectra over many orders of magnitude of scan speed.[18,19] For material designers, qualitative measurements of viscoelasticity are not always sufficient, especially as materials become more compositionally complex and the length scale of various components is continuously reduced. This has led to the development of additional AFM-based techniques and analysis to accurately determine quantitative values of properties such as the storage modulus E', loss modulus E'', and loss tangent.[20−25]

To this end, contact resonance (CR) spectroscopy methods have recently been demonstrated for the quantitative measurement of viscoelastic properties including E' and E''.[26,27] The results represent a notable extension of earlier CR spectroscopy techniques such as contact resonance force microscopy (CR-FM)[28] and atomic force acoustic microscopy[29] that have primarily been used to measure elastic properties on relatively stiff, inorganic materials. In elastic CR spectroscopy, the cantilever is flexurally excited with the tip in contact, and the shift in the resonance frequency compared to the free-space oscillation (tip out of contact) is measured. Viscoelastic CR spectroscopy also considers damping in the resonance peak to interpret a material's viscous characteristics. However, recent proof-of-concept work with CR spectroscopy did not utilize the AFM's imaging capabilities and merely involved stationary point measurements on homogeneous films. Similar to the way in which CR-FM progressed from single-point data to a quantitative imaging of the elastic modulus,[28] we now demonstrate the mapping of near-surface viscoelastic properties with CR-FM.

Received: September 1, 2011
Revised: October 7, 2011
Published: November 04, 2011

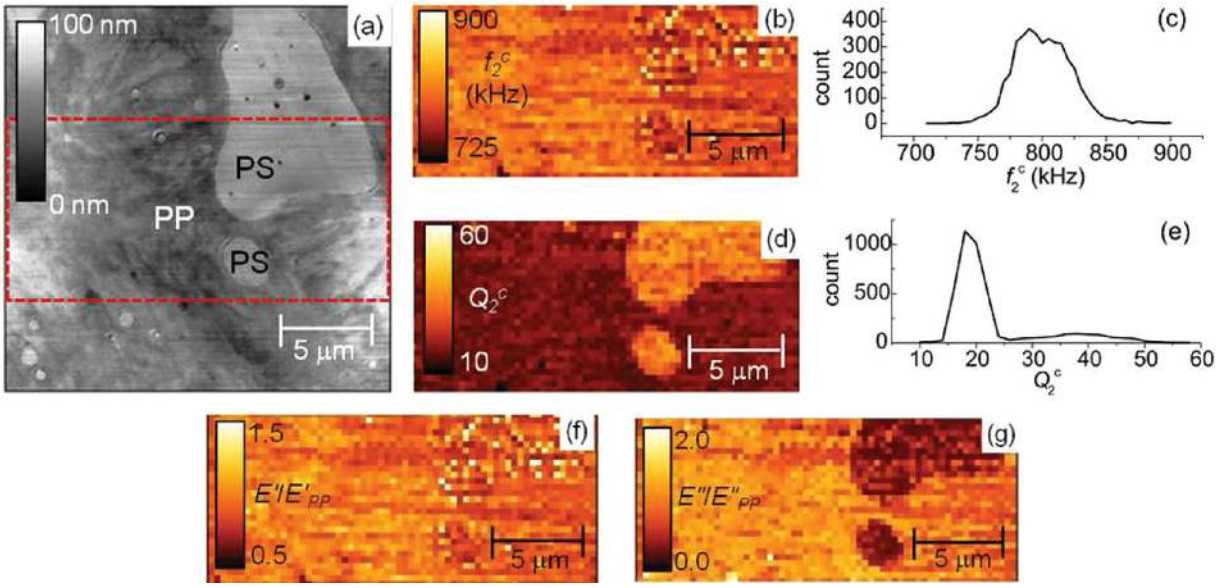

Figure 1. (a) ac-mode topography image of the PS−PP blend. Data flattened with a first-order line fit. The red box indicates the cropped regions shown in b, d, f, and g. Raw (b) f_2^c and (d) Q_2^c maps and their respective histograms, c and e. (f, g) Corresponding maps of E'/E'_{PP} and E''/E''_{PP} calculated with the viscoelastic CR-FM model.

In single-point spectroscopy with viscoelastic CR-FM,[26,27] the spectra of the free and contact resonance frequencies f_n^0 and f_n^c and the free and contact resonance quality factors Q_n^0 and Q_n^c for the nth flexural eigenmode are used to determine E' and E''. In viscoelastic CR-FM mapping, f_n^c and Q_n^c must be obtained as 2D images, and the beam mechanics analysis must be performed pixel by pixel. Analysis relies on a distributed-mass Euler-Bernoulli beam model that is expected to be accurate in the measured stiffness regime on the basis of previous experimental and theoretical work.[26,30] In free space, the damping of the cantilever is described by $\chi = 2\pi f_n^0/Q_n^0$. To consider dissipation for the tip in contact, the beam mechanics model used for elastic CR-FM analysis is modified with a Kelvin−Voigt spring-dashpot element at the tip−sample contact. Although the Voigt model oversimplifies the response of real polymeric materials, it is a useful starting point and is especially suited to describe solids.[31]

For the Kelvin−Voigt contact, the cantilever dynamics for the nth flexural eigenmode can be described with a complex normalized wavenumber $\lambda_n L = a_n + ib_n$, where L is the length of the cantilever, $a_n = x_n^0 L(f_n^c/f_n^0)^{1/2}$, and $b_n = a_n[(2\pi f_n^c - \chi Q_n^c)/8\pi f_n^c Q_n^c]$. $x_n^0 L$ is the corresponding root of the characteristic equation for free flexural vibration, $1 + \cos x_n^0 L \cosh x_n^0 L = 0$ with $x_n^0 L = (1.8751, 4.6941, 7.8548)$ for the first three modes. Thus, values of a_n, b_n, and hence $\lambda_n L$ can be determined from measurements of f_n^0, f_n^c, Q_n^0, and Q_n^c. From $\lambda_n L$, the normalized tip−sample contact stiffness α and damping coefficient β are calculated from the real and imaginary parts, respectively, of

$$\alpha + i\beta(\lambda_n L_1)^2 = \frac{\left(\frac{2}{3}\right)(\lambda_n L_1)^3[1 + \cos \lambda_n L \cosh \lambda_n L]}{[((\sinh \lambda_n L_1 \cos \lambda_n L_1 - \sin \lambda_n L_1 \cosh \lambda_n L_1)(1 + \cos \lambda_n L' \cosh \lambda_n L')) + ((1 - \cos \lambda_n L_1 \cosh \lambda_n L_1)(\sin \lambda_n L' \cosh \lambda_n L' - \cos \lambda_n L' \sinh \lambda_n L'))]} \quad (1)$$

where L_1 is the position of the AFM tip along the cantilever's length L and $L' = L - L_1$. To determine E' and E'' from α and β, a calibration approach[26,29] is used in which alternating measurements are made on both the sample of interest and one with known properties E'_{cal} and E''_{cal}.[26] Alternatively, if a heterogeneous material has a region of known (or assumed) viscoelastic properties, then it can serve as a self-calibration. By solving eq 1 for calibration values α_{cal} and β_{cal} and assuming sphere-plane Hertzian contact, the reduced storage modulus $E'^R = E'^R_{cal}(\alpha/\alpha_{cal})^{3/2}$ and reduced loss modulus $E''^R = E''^R_{cal}(f_n^c\beta/f_{n\,cal}^c\beta_{cal})^{3/2}$ for the unknown sample can be determined.[26] Finally, with a knowledge of the tip properties (and negligible damping in the tip) and assuming that Poisson's ratio ν is similar for the unknown and calibration materials, E' and E'' for the sample are extracted from the reduced complex modulus:

$$E^{*R} = E'^R + iE''^R = \left[\frac{(1-\nu^2)}{E' + iE''} + \frac{(1-\nu_{tip}^2)}{E_{tip}}\right]^{-1} \quad (2)$$

It should be noted that this analysis is developed for the case of small damping (i.e., $a_n \gg b_n$). Thus, it is most applicable to polymers in their solid states (e.g., at temperatures that are less than the glass transition or melting temperature).

EXPERIMENTAL PROCEDURE

The sample was an 80%/20% by weight melt-processed blend of polystyrene (PS) and polypropylene (PP). In preparation for AFM imaging, the sample was cryomicrotomed to ~10 nm nominal roughness and then affixed to a glass slide. The glass slide was mounted onto a broadband ultrasonic transducer (center frequency approximately 1 MHz) to provide actuation of the cantilever in contact with the sample. A wire was attached to the sample surface with silver paint and connected to the AFM chassis to dissipate electrostatic charge.

CR-FM measurements were made on an Asylum Research MFP-3D microscope with a rectangular silicon cantilever with a nominal spring constant of 3 N/m and a free resonance frequency of $f_2^0 = (451.65 \pm 0.01)$ kHz for the second flexural eigenmode. The second eigenmode was used

to maximize the sensitivity in the probed contact stiffness range.[32] The drive amplitude was set as low as possible to ensure linear tip−sample contact. Viscoelastic measurements were performed with point-by-point mapping and continuous contact-mode scanning. For all measurements, the applied force was ∼80 nN. For each pixel in the point-mapping method, the tip moves into position, the surface is engaged, a complete contact resonance spectrum is acquired, and the tip is withdrawn. A damped simple harmonic oscillator (DSHO) model is then fit to the resonance spectrum at each point to determine f_n^c and Q_n^c for that pixel.

For a contact-mode scanning-based approach, a handful of techniques exist to measure f_n^c and Q_n^c in situ;[33−35] here, we used dual ac resonance tracking (DART).[35,36] DART uses two lock-in amplifiers to acquire phase and amplitude information at frequencies on either side of the resonance peak while simultaneously tracking the resonance by adjusting the two drive frequencies.[36] By approximating the cantilever tip−sample contact by a DSHO model, images of frequency, amplitude, and phase information at each pixel are then used to calculate maps of f_n^c and Q_n^c.[35] To test the speed limits during scanning, the scan velocity v was varied from 1 to 25 μm/s.

Validation of the AFM experiments was conducted with macroscopic rheological measurements on homogeneous PP and PS specimens from the same stock that composed the blend. Storage and loss modulus values of PP and PS were determined by dynamic mechanical tensile analysis (DMTA). The DMTA measurements were performed at 1 Hz and 0.1% strain from temperatures of −100 to 150 °C. Time−temperature superposition techniques were then used to convert the temperature axis to a frequency axis for suitable comparison with the high-frequency CR measurements.

RESULTS AND DISCUSSION

Figure 1 shows point-mapping results from the PS−PP blend. As labeled in Figure 1a, the blend exhibits a continuous PP phase, with discrete PS domains ranging in size from 1 to 20 μm. The experimental point maps in Figure 1b,d reveal that the PS−PP blend exhibits little frequency contrast but a large quality factor contrast. The contact resonance frequencies were f_2^c = (792.1 ± 31.7) kHz and f_2^c = (801.7 ± 17.4) kHz for the PS and PP regions, respectively. The corresponding quality factors were Q_2^c = 37.3 ± 5.0 and 18.4 ± 2.7 for the PS and PP regions, respectively. The uncertainty in f_2^c and Q_2^c represents one standard deviation in the data for the indicated phases and a significant source of uncertainty in the determination of modulus values. As seen in the histograms in Figure 1c,e, the small f_2^c contrast and large Q_2^c contrast suggest that qualitatively the two phases have similar elastic stiffnesses but different damping characteristics.

Because the true damping is a function of both the frequency and quality factor, a quantitative evaluation of the stiffness and damping requires further analysis.[3] The viscoelastic CR-FM analysis approach summarized above was used on the data in Figure 1b,c to calculate images of the contact stiffness α and damping β. Then, from Figure 1b and the images of α and β, maps were calculated of the relative storage modulus E'/E'_{PP} and loss modulus E''/E''_{PP}. These maps are shown in Figure 1d,e, respectively. To calculate the images, the viscoelastic properties of the polypropylene phase were assumed to be those of bulk homogeneous polypropylene. The tip properties were assumed to be those of ⟨100⟩ silicon. Values for α_{cal}, β_{cal}, and $f_2^c{}_{cal}$ were determined from masked averages of the PP phase in the α, β, and f_2^c maps.

An analysis of the images in Figure 1d,e yielded an average value of E'_{PS}/E'_{PP} = 0.95 ± 0.20 for the polystyrene−polypropylene storage modulus ratio, and E''_{PS}/E''_{PP} = 0.34 ± 0.16 for the loss modulus ratio. For comparison, we performed dynamic mechanical tensile analysis (DMTA) on homogeneous (bulk) PP and PS specimens that corresponded to the individual phases from the blend. To account for any frequency dependence of the viscoelastic properties, time−temperature−superposition (TTS) analysis was used to shift the low-frequency (∼1 Hz) DMTA data into the high-frequency (∼1 MHz) regime probed by CR-FM. This approach does not ensure comparable strain rates but does provide baseline high-frequency loss and storage modulus ratios for validation. From the TTS analysis, we predict E'_{PS}/E'_{PP} = 0.85 and E''_{PS}/E''_{PP} = 0.37 at 1 MHz, in good agreement with our CR-FM results.

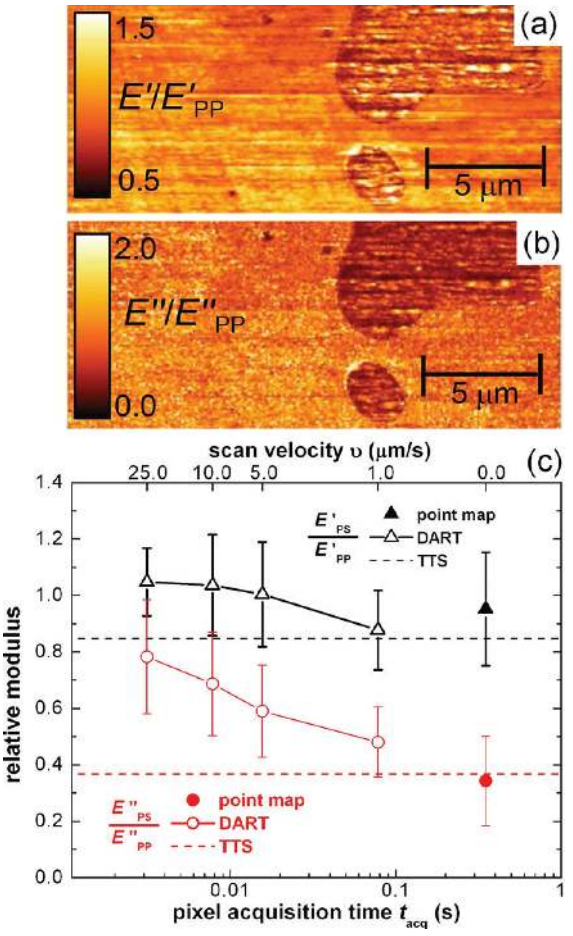

Figure 2. Viscoelastic maps of relative modulus (a) E'/E'_{PP} and (b) E''/E''_{PP} obtained with DART contact scanning for a scan velocity v = 1 μm/s. (c) Calculated storage modulus ratio (black) and loss modulus ratio (red) versus v and pixel acquisition time t_{acq}. Dashed lines indicate bulk predictions from time−temperature superposition analysis.

It has been reported elsewhere that the surface mechanical properties of polymers can vary considerably from those of the bulk.[19,37,38] For example, the polymer mobility can be increased at the free surface,[19,37] or the tip−sample contact can induce molecular confinement.[38] The fact that our viscoelastic CR-FM results agree so well with bulk values suggests that the applied force (∼80 nN) was sufficiently large that measurements were dominated by bulklike material. Assuming Hertzian contact mechanics and homogeneous material, we estimate that our experimental conditions result in a stress field that is most sensitive to material down to ∼30 nm below the surface. Something like a mobile surface layer in polystyrene is expected to be compliant and only a few nanometers thick;[37] thus, its effect

dx.doi.org/10.1021/la203434w |Langmuir 2011, 27, 13983–13987

may be negligible in the present experiments. It is also possible that the microtoming process yielded surface material in a more bulklike state than that obtained from casting techniques with an annealing step.

The good agreement between the viscoelastic CR-FM results and bulk DMTA values is also notable in light of the simplified contact mechanics model implemented. We have assumed Hertzian contact in which only elastic forces are considered. The Hertz model seems to be an appropriate starting point because the experimental tip−sample adhesion forces were much smaller than the applied force and of comparable magnitude for the two phases. Measurements made at lower applied forces or on materials with dramatically higher adhesion forces would require analysis with a more advanced contact model such as the Derjaguin−Müller−Toporov[39] or Johnson−Kendall−Roberts[40] models.

The primary limitation of the point-mapping scheme above is its slow speed. In the current implementation, it takes ∼2 s to acquire each pixel. Thus, a low-resolution image (64 pixels × 64 pixels) requires ∼140 min, and the acquisition time scales linearly with the total number of pixels. To achieve faster, higher-resolution viscoelastic CR-FM mapping, we investigated a scanning-based acquisition approach.

Figure 2a,b shows the relative viscoelastic property maps obtained at v = 1 μm/s. The maps are similar in contrast to those in Figure 1d,e, but the spatial resolution is much greater. Even at such a slow velocity, scanning enabled a 16-fold increase in pixel resolution compared to the point map, at the cost of only 50% more imaging time. Increasing the scan velocity led to even shorter imaging times; however, we observed that the image contrast and quality were adversely affected by faster scanning. These results are summarized together with the point map and bulk results in Figure 2c. To compare measurement timescales between DART and point mapping, the data in Figure 2c are plotted versus the duration of time t_{acq} to acquire a single pixel and the scan velocity v. For the point-mapping results, it should be noted that the duration of contact time preceding and during acquisition can affect values of f_n^c and Q_n^c. Consistent with the point-mapping results, it can be seen that the storage modulus ratio E'_{PS}/E'_{PP} is close to unity for all scan speeds in DART mode. The loss modulus ratio shows a more pronounced trend versus t_{acq} and v. For all values of v, the E''_{PS}/E''_{PP} results consistently resolve polypropylene as exhibiting more damping than polystyrene, thus capturing the expected qualitative trend. The goodness of quantitative agreement for E'' among scanning measurements, point maps, and bulk measurements was speed-dependent and improved at lower scan velocities. For v = 1.0 μm/s, $E''_{PS}/E''_{PP} = 0.48 \pm 0.12$, showing reasonable agreement with the bulk prediction $E''_{PS}/E''_{PP} = 0.37$.

Possible reasons for the scan speed dependence of the modulus ratios include material, contact mechanics, and instrumentation effects. Concerning material effects, it has been shown that the scan velocity can be used to probe the frequency-dependent viscoelastic properties of a material.[18,19,41] This effect is complicated by the selective frequency regime probed by CR-FM. Overall, for a heterogeneous material containing phases with different frequency dependences (e.g., because of its proximity to thermal transitions, variations in polymer structure, or the presence/absence of a water layer), the calculated modulus ratio could differ with the scan velocity. Regarding contact mechanics, scanning may affect the tip−sample contact area. In maps of f_2^c for a single region, we observed a systematic decrease in frequency with an increased scan velocity. Changes in f_n^c during scanning have been shown to relate directly to changes in contact area[42] and may stem from reduced adhesive contributions during sliding versus static contact.[43] Finally, concerning instrumentation effects, faster scanning in the presence of topographic features may induce some nonideality in the resonance peak. Also, the DART peak-tracking feedback loop may lag behind the topography when imaging at faster scan velocities. In such scenarios, the measurements are noisy because they are taken at frequencies away from resonance. The combined instrumentation effects could result in less-accurate Q_n^c data or data that are discarded because they violate the DSHO model assumptions. In our results, faster scanning led to greater data scatter and an increased number of pixels with discarded data, consistent with the presence of these effects.

In summary, we have demonstrated that viscoelastic CR-FM mapping provides spatially resolved quantitative images of the conservative and dissipative properties of materials. The approach relies on accurate measurements of the contact resonance frequency and quality factor as the tip moves across the sample in either a point-mapping or continuous-scanning configuration. With current equipment and analysis models, point mapping and slow scanning provide the most consistent and robust quantitative information, particularly for dissipative quantities. Imaging of the loss and storage modulus at faster scan rates can yield qualitatively similar property information with impressively shortened acquisition times. This may be necessary for samples that age rapidly and may be used to mitigate the effects of thermal drift. Scanning-based approaches are also well suited for rapid-throughput applications in which specific regions of interest could be identified with faster scanning and then finely probed with slow scanning or point mapping. Overall, the quantitative nature of viscoelastic CR-FM will enable a deeper understanding of the near-surface, high-frequency viscoelastic response of heterogeneous nanostructured polymers and other materials.

AUTHOR INFORMATION

Present Addresses

⊥Current address: Department of Mechanical and Aerospace Engineering, Clarkson University, Potsdam, New York 13699, United States.

ACKNOWLEDGMENT

We acknowledge J. Grabowski (ExxonMobil) for sample preparation and M. Amin (ExxonMobil) for the DMA results. J.A.T. and P.A.Y. acknowledge the support of the NSF (grant nos. EPS-0701892 and CMMI-0709333). This research was performed while J.P.K. held an NRC Research Associateship Award at NIST. The mention of commercial products does not imply recommendation or endorsement by NIST.

REFERENCES

(1) Binnig, G.; Quate, C. F.; Gerber, C. *Phys. Rev. Lett.* **1986**, *56*, 930–933.

(2) Du, B.; Tsui, O. K. C.; Zhang, Q.; He, T. *Langmuir* **2001**, *17*, 3286–3291.

(3) Rezende, C. A.; Lee, L.-T.; Galembeck, F. *Langmuir* **2009**, *25*, 9938–9946.

(4) Bar, G.; Thomann, Y.; Brandsch, R.; Cantow, H. J.; Whangbo, M. H. *Langmuir* **1997**, *13*, 3807–3812.

(5) Butt, H. J.; Cappella, B.; Kappl, M. *Surf. Sci. Rep.* **2005**, *59*, 1–152.

(6) Garcia, R.; Perez, R. *Surf. Sci. Rep.* **2002**, *47*, 197–301.
(7) Schon, P.; Bagdi, K.; Molnar, K.; Markus, P.; Pukanszky, B.; Vancso, G. J. *Eur. Polym. J.* **2011**, *47*, 692–698.
(8) Sahin, O.; Magonov, S.; Su, C.; Quate, C. F.; Solgaard, O. *Nat. Nanotechnol.* **2007**, *2*, 507–514.
(9) Garcia, R.; Magerle, R.; Perez, R. *Nat. Mater.* **2007**, *6*, 405–411.
(10) Holscher, H. *Appl. Phys. Lett.* **2006**, *89*, 3.
(11) Attard, P. *J. Phys.: Condens. Matter* **2007**, *19*, 473201.
(12) McConney, M. E.; Singamaneni, S.; Tsukruk, V. V. *Polym. Rev.* **2010**, *50*, 235–286.
(13) Tamayo, J.; García, R. *Langmuir* **1996**, *12*, 4430–4435.
(14) Kajiyama, T.; Tanaka, K.; Ohki, I.; Ge, S.-R.; Yoon, J.-S.; Takahara, A. *Macromolecules* **1994**, *27*, 7932–7934.
(15) Radmacher, M.; Tilmann, R. W.; Gaub, H. E. *Biophys. J.* **1993**, *64*, 735–742.
(16) Chizhik, S. A.; Gorbunov, V. V.; Luzinov, I.; Fuchigami, N.; Tsukruk, V. V. *Macromol. Symp.* **2001**, *167*, 167–175.
(17) Moeller, G. *J. Polym. Sci., Part B: Polym. Phys.* **2009**, *47*, 1573–1587.
(18) Haugstad, G.; Gladfelter, W. L.; Weberg, E. B.; Weberg, R. T.; Jones, R. R. *Langmuir* **1995**, *11*, 3473–3482.
(19) Tanaka, K.; Takahara, A.; Kajiyama, T. *Macromolecules* **1997**, *30*, 6626–6632.
(20) Fretigny, C.; Basire, C.; Granier, V. *J. Appl. Phys.* **1997**, *82*, 43.
(21) Mahaffy, R. E.; Park, S.; Gerde, E.; Käs, J.; Shih, C. K. *Biophys. J.* **2004**, *86*, 1777–1793.
(22) McGuiggan, P. M.; Yarusso, D. J. *J. Mater. Res.* **2004**, *19*, 387–395.
(23) Xu, W.; Wood-Adams, P. M.; Robertson, C. G. *Polymer* **2006**, *47*, 4798–4810.
(24) Minary-Jolandan, M.; Yu, M.-F. *Ultramicroscopy* **2008**, *108*, 821–825.
(25) Yang, N.; Wong, K. K. H.; de Bruyn, J. R.; Hutter, J. L. *Meas. Sci. Technol.* **2009**, *20*, 025703–025703.
(26) Yuya, P. A.; Hurley, D. C.; Turner, J. A. *J. Appl. Phys.* **2008**, *104*, 074916–074916.
(27) Yuya, P. A.; Hurley, D. C.; Turner, J. A. *J. Appl. Phys.* **2011**, *109*, 113528.
(28) Hurley, D.; Kopycinska-Müller, M.; Kos, A. *JOM* **2007**, *59* (1), 23–29.
(29) Rabe, U.; Amelio, S.; Kopycinska, M.; Hirsekorn, S.; Kempf, M.; Goken, M.; Arnold, W. *Surf. Interface Anal.* **2002**, *33*, 65–70.
(30) Rabe, U.; Turner, J.; Arnold, W. *Appl. Phys. A: Mater. Sci. Process.* **1998**, *66*, S277–S282.
(31) Benbow, J. J.; Cogswell, F. N.; Cross, M. M. *Rheol. Acta* **1976**, *15*, 231–237.
(32) Turner, J. A.; Wiehn, J. S. *Nanotechnology* **2001**, *12*, 322–330.
(33) Yamanaka, K.; Maruyama, Y.; Tsuji, T.; Nakamoto, K. *Appl. Phys. Lett.* **2001**, *78*, 1939–1941.
(34) Jesse, S.; Kalinin, S. V.; Proksch, R.; Baddorf, A. P.; Rodriguez, B. J. *Nanotechnology* **2007**, *18*, 435503–435511.
(35) Gannepalli, A.; Yablon, D. G.; Tsou, A. H.; Proksch, R. *Nanotechnology* **2011**, *22*, 355705–355705.
(36) Rodriguez, B. J.; Callahan, C.; Kalinin, S. V.; Proksch, R. *Nanotechnology* **2007**, *18*, 475504–475510.
(37) Keddie, J. L.; Jones, R. A. L.; Cory, R. A. *Europhys. Lett.* **1994**, *27*, 59–64.
(38) Tweedie, C. A.; Constantinides, G.; Lehman, K. E.; Brill, D. J.; Blackman, G. S.; Van Vliet, K. J. *Adv. Mater.* **2007**, *19*, 2540–2546.
(39) Derjaguin, B. V.; Muller, V. M.; Toporov, Y. P. *J. Colloid Interface Sci.* **1975**, *53*, 314–326.
(40) Johnson, K. L.; Kendall, K.; Roberts, A. D. *Proc. R. Soc. London, Ser. A* **1971**, *324*, 301–313.
(41) Sills, S.; Gray, T.; Overney, R. M. *J. Chem. Phys.* **2005**, *123*, 134902–134908.
(42) Killgore, J. P.; Geiss, R. H.; Hurley, D. C. *Small* **2011**, *7*, 1018–1022.
(43) Johnson, K. L. *Proc. R. Soc. London, Ser. A* **1997**, *453*, 163–179.